Drag force in a cold or hot granular medium

A. Seguin[1,2] and P. Gondret[1]

[1]*Laboratoire FAST, Université Paris-Sud, CNRS, Université Paris-Saclay, F-91405, Orsay, France*
[2]*SPEC, CEA, CNRS, Université Paris-Saclay, F-91191 Gif-sur-Yvette, France*

We measure experimentally and analyze the resisting force exerted by a bidimensional packing of small disks on a larger intruder disk dragged horizontally at constant velocity V_0. Depending on the vibration level of the packing that leads to a granular "cold" or "hot" packing, two force regimes are observed. At low vibration level ("cold" granular medium), the drag force F does not depend on V_0, whereas for high vibrations ("hot" granular medium), the drag force increases linearly with V_0. Both regimes can be understood by the balance of two "granular temperatures" that can be defined in the system: a bulk temperature T_b imposed by the external vibration to the overall packing and a local temperature T_0 induced by the own motion of the intruder disk in its vicinity. All experimental data obtained for different sizes and velocities of the intruder disk are shown to be governed by the temperature ratio T_0/T_b. A critical velocity V_{0c}, above which the system switches from "hot" to "cold," can be obtained in this frame. Finally, we discuss how these two "viscous" regimes should be followed by an inertial regime where the drag force F should increase as V_0^2 at high enough velocity values, for V_0 greater than a critical value V_{0i} corresponding to high enough Reynolds or Froude number.

I. INTRODUCTION

The mechanical response of a granular material under a global or local stress is a fundamental issue in many industrial fields, such as civil engineering and pharmaceutics, but also environmental fields. In particular, the response to a local forcing from a moving object is important, for instance, in soil mechanics for pile driving [1], in geophysics and astrophysics for the impact of meteorites [2], and in biophysics or robotics for the understanding of the locomotion of animals on or through sand [3]. Despite key advances in the granular description, the complete rheology of granular materials remains a challenging problem: it is still worth understanding its complexity, especially close to the so-called "liquid-solid transition" characterized by a "jamming" value [4–6]. Above this transition, granular matter behaves like a (complex) liquid that tends to flow under an applied stress. In these athermal systems, (weak) external vibrations may affect drastically the rheological curves [7]. More generally, granular matter belongs to the same class of materials as glass-forming liquids or colloidal suspensions. These disordered materials are the head of dynamical heterogeneities which are nonlocal processes [8]. These nonlocal processes causing diffusion through the system have to be implemented in the rheology of granular materials. In recent years, several models have been proposed to take them into account via the concept of granular fluidity [9,10], the $\mu(I)$ rheology in its nonlocal form [11,12], or kinetic theory applied to dense flows [13,14].

The complex rheology of granular materials makes the understanding of the generated drag force on a sphere or a cylinder difficult [15]. In such a situation, the difficulty arises from the nonparallel flow in contrast with simpler flow situations, such as the Couette flow between two parallel plates or the gravity flow of a layer of constant thickness down an incline. Many experiments and numerical studies have been carried out recently to characterize the drag force on either a cylinder [15–26] or a sphere [27–30], or on an object of more complex shapes [31] in translation through grains. The influence of an externally driven fluidization of the granular material has been investigated either with wall vibrations [20,27,32] or sound waves [28] or from the steady motion of a far wall [33–35]. Different scalings of the drag force with the relative velocity of the object have been reported in all these studies. At very high velocity, the drag force increases as the square of the velocity as in the inertial hydrodynamic regime corresponding to large Reynolds numbers for Newtonian fluids [19,21,29,30]. At low velocity, the drag force is generally independent of the velocity V_0 [16,18], but experiments with a granular material "fluidized" by an external forcing may lead to a linear dependence of the drag force with the velocity [27] as in the viscous hydrodynamic regime corresponding to low Reynolds numbers for Newtonian fluids. Other studies with external fluidization forcing report also some weak velocity dependence of the drag force, which may appear as logarithmic [20,28]. These observed scaling laws thus need some clarification, in particular, the role played by external or internal fluidization.

In this paper, we focus on the transition from a velocity-independent regime to a linear velocity regime of the drag force, with an experimental setup consisting of an intruder disk dragged at different velocities in a horizontal packing of disks that can be shaken horizontally, contrary to most of the previous studies [27,28,32], where the vibrations were vertical. Measurements of the drag force are here analyzed in terms of the balance of two granular temperatures: one external temperature T_b imposed by the vibration of the bottom wall to the overall packing and another temperature T_0 locally induced by the motion of the intruder disk. A hydrodynamic model, based on kinetic theory, is developed taking into account the two sources of fluidization that allow to recover the transition between the two regimes.

II. EXPERIMENTAL SETUP

The present experimental setup is adapted from a previous one already used by Refs. [20,36]. The granular assembly is
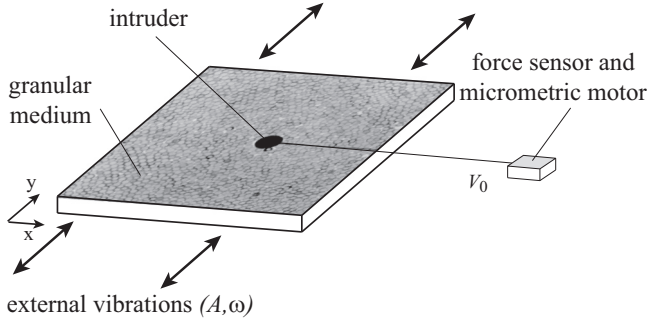
intruder

granular
medium

force sensor and
micrometric motor

V_0

y

x

external vibrations *(A,ω)*

FIG. 1. Sketch of the experimental setup.

composed of about $N \simeq 8 \times 10^3$ polyurethane (PSM4) disks of density $\rho_s = 1280$ kg/m^3, height 3.2 mm, and diameters 4 and 5 mm, with a bidisperse size distribution to avoid any crystallization. This disk assembly of average diameter $d_g = 4.5$ mm is placed on a horizontal bottom plate within a square area of side $L = 400$ mm delimitated by side walls, which are fixed in the laboratory frame (Fig. 1). Another horizontal glass plate mounted above prevents the disks from going out the bidimensional plane assembly and allow visualization from above. The packing fraction $\phi = N\pi(d_g/2L)^2$ is here fixed to $\phi = 0.80$ and corresponds to a dense packing without prestress below the jamming value, which corresponds here to $\phi_J \simeq 0.825$ [5]. A larger intruder disk of diameter $d = 8$, 16, or 32 mm (made in aluminium) is initially placed at one side of the square box around the position $(x,y) \simeq (L/3,L/2)$, is then pulled by a steel wire at the constant velocity V_0 in the x direction toward the opposite side at the final position around $(2L/3,L/2)$, with a controlled displacement deck in the range $10^{-4} < V_0 < 3$ mm.s^{-1}. The bottom plate can be vibrated horizontally in the y direction perpendicular to the intruder motion at a given frequency ω and amplitude A, which are fixed to $\omega/2\pi = 10$ Hz and $A = 10$ mm. The vibration amplitude A has been chosen to be much larger than the typical interstitial gap $s \simeq [(\phi_J/\phi)^{1/2} - 1]d_g$ between the disks, to

generate fluctuations in the disk positions within the overall packing. As a matter of fact, the mechanical vibration does not concern here all the container but only the bottom wall, whereas the sidewalls are fixed. The onset of time fluctuations in the relative disk positions is thus not governed by the acceleration ratio $A\omega^2/g$, as in the classical vibration of the overall container, but is governed here by the size ratio A/s. In the case where $A/s \gg 1$, here $A/s \simeq 10^2$, disk fluctuations exist in the system and do not depend on A but only on $s(\phi)$ and ω [37]. The instantaneous drag force $F(t)$ exerted by the disk assembly on the moving intruder disk is measured with a piezoelectric sensor to which the wire is attached. Before the intruder motion, the whole packing is homogenized by a slight vibration of the bottom plate of the cell. During the intruder motion, the bottom plate is either vibrating or not while the drag force F is recorded as a function of time t.

III. EXPERIMENTAL RESULTS

A typical drag force signal $F(t)$ is shown in Fig. 2(a). In the case of no external vibration [$\omega = 0$, - - - in Fig. 2(a)], the drag force $F(t)$ exhibits strong and rapid fluctuations, which may be associated to the formation and breakage of long force chains. But the force signal does not show any significant evolution along the intruder path so that we can consider that a stationary regime is reached and characterized by a constant drag force with the time averaged value $F = \overline{F(t)} \simeq 0.3$ N (where $\overline{\cdot}$ is time-averaging) in the case of Fig. 2(a). These observations are in agreement with previous experiments [15]. In the presence of external vibrations [$\omega \simeq 63$ s^{-1}, — in Fig. 2(a)], the force fluctuations are much smaller which suggests that the system does not promote long force chains anymore. Despite a slow time increase of the drag force along the intruder path, as a first step we will consider only its time averaged value [$F \simeq 0.15$ N in the case of Fig. 2(a)] in the following. This slight increase is due to the convection that arises from a large recirculation roll of weak velocity in the overall cell. Such convection has already been reported by Ref. [37] in a very
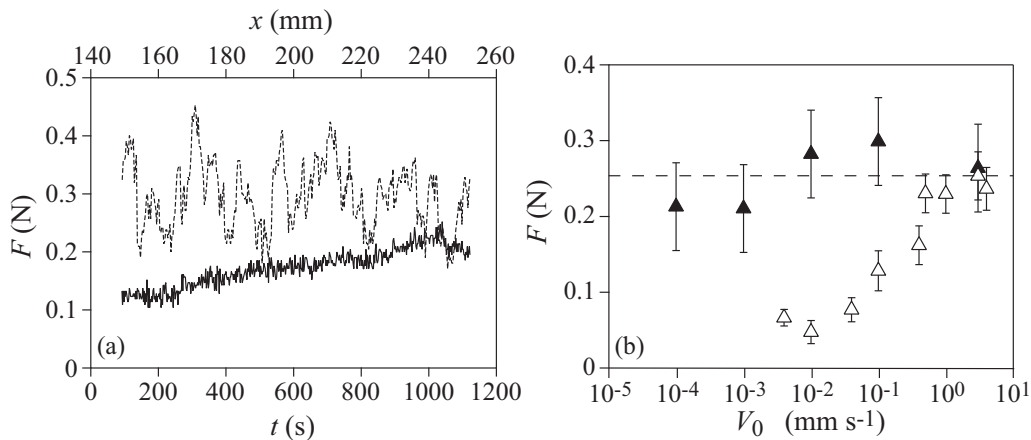

FIG. 2. (a) Evolution of the instantaneous drag force F as a function of time t and disk position x for an intruder disk of diameter $d = 8$ mm at velocity $V_0 = 0.1$ mm.s^{-1} in the case of no external vibrations ($\omega = 0$, - - -) or external vibrations ($\omega \simeq 63$ s^{-1}, —) of a granular packing of solid fraction $\phi = 0.80$. (b) Drag force F as a function of velocity V_0 (a) without packing vibrations (▲, $\omega = 0$) and (b) with packing vibration (△, $\omega \simeq 63$ s^{-1}) for an intruder disk of diameter $d = 8$ mm in a granular packing of solid fraction $\phi = 0.80$. (- - -) Mean value $F_0 = 0.25$ N for $\omega = 0$. The error bars correspond to the standard deviation of the drag force signal $F(t)$.

similar set up and by Ref. [38] in fluidized beds. When the intruder is dragged here from one side of the cell to the other, it passes across the convection roll which slightly modifies the drag force, which is underestimated at low value of x and overestimated at high value of x [Fig. 2(a)], so that we expect that the force average along the path is the correct one. That is also why it would be reckless to carry out experiments below $V_0 \simeq 4 \times 10^{-3}$ mm.s^{-1} with vibrations: In this case the intruder would not follow a straight line anymore. One can see in Fig. 2(a) that the mean value of the drag force is significantly smaller in presence of external vibrations which suggests a global fluidization of the packing. In the following we will focus on the mean drag force averaged over the distance $\Delta x = 120$ mm smaller that the total distance $2L/3 \simeq 270$ mm traveled by the intruder, by removing carefully the starting transient and the end part to be far enough from the approaching wall [39]. Figure 2(b) shows all F data as a function of the intruder velocity V_0 with and without external vibrations. Without external vibration ($\omega = 0$, filled symbols), the drag force does not depend on the intruder velocity as already observed in many experiments [15,16,23,24,40]. With external vibrations ($\omega \simeq 63$ s^{-1}, open symbols), the drag force is always smaller than in the case of no vibration, and increases with the velocity as also reported by some studies [27,28]. Let us now understand these two different behaviors within the frame of a single hydrodynamical model taking into account two fluctuations sources in terms of two granular temperatures.

IV. HYDRODYNAMICAL MODEL

The classical kinetic theory for molecular systems has been applied with some success to dilute and even dense athermal granular systems by introducing the concept of a "granular temperature" T linked not to the mean grain velocity $\bar{v}$ but to the mean velocity fluctuations: $T = \overline{(v - \bar{v})^2}$. In the present case of external vibrations with the horizontal shaking of the bottom wall only, fluctuations are generated in the overall packing at the external forcing frequency ω but with typical displacements limited to the mean distance $s = [(\phi_J/\phi)^{1/2} - 1]d_g$ between disks, as the system would jam for $\phi = \phi_J$ without any relative disk motion. The characteristic bulk granular temperature induced by the external vibration of the overall packing should thus be given by $T_b = V_b^2$, where $V_b \sim s\omega \sim [(\phi_J/\phi)^{1/2} - 1]d_g\omega$ is expected to be the typical velocity magnitude of the fluctuation in the overall packing.

Without external vibration, in a slightly different configuration of a circular cylinder moving perpendicularly to its axis within a dense packing of beads, PIV measurements have shown that a zone of high temperature T_0 exists in a narrow crown of extension λ around the cylinder, inducing a strongly localized flow herein [23,24]. The corresponding local temperature in this narrow crown has been shown to scale as $T_0 = V_0^2 d_g/d$. This scaling, which implies the cylinder/grain size aspect ratio d/d_g has been observed in a quasi bidimensional configuration with $d/d_g > 1$, so that we consider the same scaling in the present bidimensional configuration of a large intruder disk within smaller disks.

In kinetic theory of granular systems, the effective viscosity η is related to the granular temperature T through $\eta = \eta_0 p d_g T^{-1/2}$, where p is the pressure and η_0 a numerical
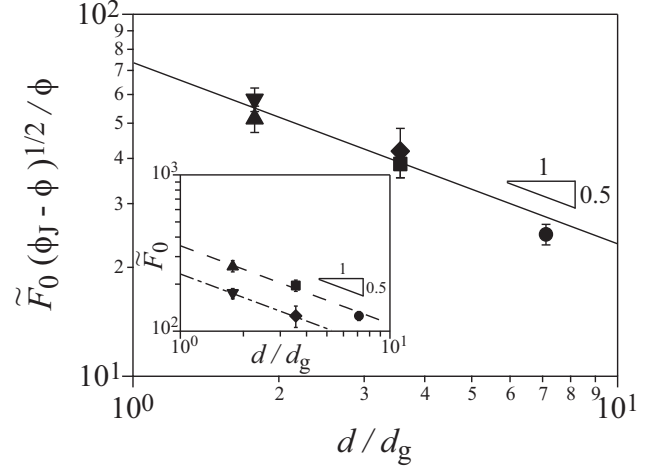

FIG. 3. Normalized drag force $\tilde{F}_0(\phi_J - \phi)^{1/2}/\phi$ without packing vibrations ($\omega = 0$) as a function of the size ratio d/d_g. Measurements for an intruder disk of diameter $d = 8$ mm (▲), 16 mm (■), and 32 mm (●) in a granular medium of solid fraction $\phi = 0.80$, and for $d = 8$ mm (▼) and $d = 16$ mm (♦) in a less dense packing $\phi = 0.76$ together with the model equation $\tilde{F}_0(\phi_J - \phi)^{1/2}/\phi = 73(d/d_g)^{-1/2}$ (—). Inset : Same data for the normalized drag force $\tilde{F}_0 = F_0/\rho_s g h^2 d$ with the model equations $\tilde{F}_0 = 350(d/d_g)^{-1/2}$ (- - -) for $\phi = 0.80$ and $\tilde{F}_0 = 230(d/d_g)^{-1/2}$ (− · −) for $\phi = 0.76$.

constant of order unity [23,41–43]. The drag force F on an object of size d that can be inferred from this hydrodynamic approach thus comes from the local viscous stresses around the cylinder that scale as $\eta\dot{\gamma}$ where $\dot{\gamma}$ is the local shear rate.

In nonvibrated granular matter, the flow has been shown by Refs. [23,24,44] to be localized close to the moving cylinder with a characteristic length λ that depends on both the intruder size d and the grain size d_g [24]. The shear rate around the cylinder being $\dot{\gamma} \sim V_0/\lambda$, the drag force F_0 on the present cylindrical intruder of height h should thus scale as $F_0 \sim \eta V_0 h d/\lambda$. Considering the typical temperature $T_0 = V_0^2 d_g/d$ around the moving cylinder and the corresponding viscosity η, the drag force should thus scale as $F_0 \sim phd^{3/2}d_g^{1/2}/\lambda$ with no more dependence upon V_0 as reported in many experiments [16,23,24,40]. In standard experiments, the pressure p in general induced by gravity with the typical hydrostatic pressure scaling $\rho_s g h$ weighted by a function of the solid fraction $f(\phi)$, so that the scaling for the drag force on the cylinder of surface $\sim hd$ should be $F_0 \sim f(\phi)\rho_s g h^2 d^{3/2}d_g^{1/2}/\lambda$. The h^2 dependance is indeed often reported from measurements, e.g., by Refs. [16,25]. The final scaling of the force F_0 with the intruder diameter d and the grain diameter d_g is not as simple because the flow length scale λ depends on both d and d_g. Indeed, the reported scaling from measurements varies from one study to the other [16,24,28]. In our 2D horizontal granular layer, the pressure scaling is also given by $f(\phi)\rho_s g h$ due to the solid friction at the bottom wall related to the grain weight $\sim \rho_s g h d_g^2$ and acting on the grain surface $\sim d_g^2$, so that we expect the same scaling law for the drag force F_0 as for the standard 3D situations with many grain layers. Our measurements made for different intruder sizes d and grain sizes d_g and reported in the inset of Fig. 3

show that the normalized drag force $\tilde{F}_0 = F_0/\rho_s gh^2 d$ scales as $(d/d_g)^{-1/2}$, which implies that $\lambda \sim d$. It is not surprising that $\tilde{F}_0$ depends also on the solid fraction ϕ with lower values for lower ϕ as also shown in the inset of Fig. 3. $\tilde{F}_0$ is expected to increase with ϕ and to diverge when approaching the jamming point ϕ_J as shown by the bidimensional experiments of Ref. [30], where the scaling $f(\phi) = \phi(\phi_J - \phi)^{-1/2}$ is proposed. In our case, the same scaling for $f(\phi)$ works quite well as data points for the different ϕ collapse onto the same curve $\tilde{F}_0/\phi(\phi_J - \phi)^{-1/2} \simeq 73(d/d_g)^{-1/2}$ as shown in Fig. 3. As a conclusion, the drag force in the nonvibrated granular matter case scales as

$$F_0 \sim \rho_s gh^2 d^{1/2} d_g^{1/2} \phi(\phi_J - \phi)^{-1/2}. \qquad (1)$$

In the case of a vibrated packing ($\omega \neq 0$), granular fluctuations around the moving intruder come both from the own intruder motion and the external vibration. With a heuristic approach, we will consider that the local temperature around the intruder is roughly given by a weighted combination of the two temperatures T_0 and T_b: $T \sim T_0 + \alpha^2 T_b$, with an unknown weighting factor α. The ratio of the local temperature T around the moving intruder for a vibrated packing relative to its value T_0 without vibration would be given in this case by

$$\frac{T}{T_0} \sim 1 + \frac{\alpha^2[(\phi_J/\phi)^{1/2} - 1]^2 dd_g \omega^2}{V_0^2} \sim 1 + \frac{V_{0c}^2}{V_0^2}. \qquad (2)$$

In this simple view, the temperature around the intruder depends on the intruder velocity relative to a critical velocity $V_{0c} \sim \alpha[(\phi_J/\phi)^{1/2} - 1](dd_g)^{1/2}\omega$.

The corresponding drag force F in a vibrated packing relative to its value F_0 in a nonvibrated packing is thus given by

$$\frac{F}{F_0} \sim \left(\frac{T_0}{T}\right)^{1/2} \sim \frac{V_0}{V_{0c}[1 + (V_0/V_{0c})^2]^{1/2}}. \qquad (3)$$

According to this expression, the drag force in a vibrated packing should increase first linearly with V_0 at low enough velocity ($V_0/V_{0c} < 1$) before saturating progressively at larger velocity to its value F_0 corresponding to no vibration.

V. DISCUSSION

Let us now compare the experimental data to the predictions of this hydrodynamic model. Figure 4 shows the evolution of the normalized drag force F/F_0 as a function of the normalized velocity V_0/V_{0c}. All the experimental data collapse on the model curve, which clearly shows the drag increase in a "hot" granular medium and its plateau value in a "cold" granular medium. The best fit is obtained for the fitting parameter value $\alpha \simeq 0.02$.

All possible regimes of drag force in granular media can thus be summarized in the diagram of Fig. 5 for increasing velocity, with two possible different "viscous" regimes followed by an ultimate inertial regime. When the intruder velocity V_0 is smaller than a critical velocity V_{0c} that depends on the vibration amplitude, the drag force increases linearly with V_0 in a so-called "hot granular viscous regime." Here the fluidization induced by the intruder motion is negligible compared to the fluidization of the overall packing [Eq. (3) for
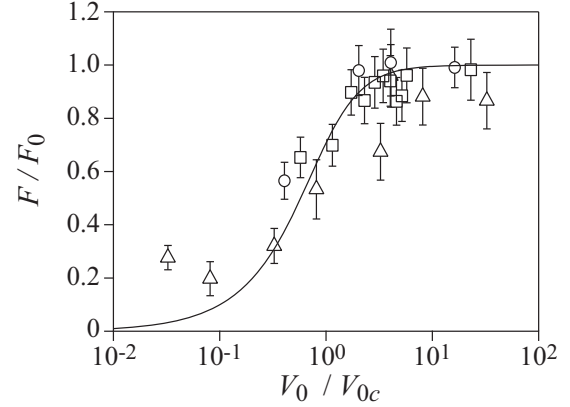

FIG. 4. Normalized drag force $F^\star = F/F_0$ as a function of the normalized velocity $V^\star = V_0/V_{0c}$ in a granular medium of solid fraction $\phi = 0.80$ vibrated at $\omega \simeq 63$ s^{-1} for an intruder diameter $d = 8$ mm ($\triangle$), 16 mm ($\square$), or 32 mm ($\circ$). (- - -) Fitting curve of equation $F^\star = V^\star/[1 + V^{\star 2}]^{1/2}$ with $\alpha = 0.02$ in the expression of V_{0c}.

$V_0 \ll V_{0c}$]. When $V_0 > V_{0c}$, the drag force does not depend on V_0 anymore in a so-called "cold granular viscous regime." Here the fluidization induced by the overall packing is negligible compared to the fluidization induced by the motion of the intruder [Eq. (3) for $V_0 \gg V_{0c}$]. In this second regime, the scaling of the force should be the one of Eq. (1). This regime corresponds to most of the standard experimental situations and is expected to be followed by an "inertial regime" at even larger intruder velocity. In that last regime, above another critical velocity V_{0i}, the drag force then increases as V_0^2. In classical hydrodynamics the viscous-inertial transition is governed by the Reynolds Re $= \rho V_0 d/\eta$ number with the critical value Re$_c \sim 1$ and thus a critical velocity that scales as $V_{0i} \sim \eta/\rho d$. In the granular case, with the corresponding expression for the effective viscosity η, the critical velocity V_{0i} is thus expected to scale as $V_{0i} \sim (gh)^{1/2}(d_g/d)^{1/4}$. As the effective viscosity in granular systems is related to pressure contrary to Newtonian fluids, the corresponding critical velocity depends on the depth h. A relation thus exists between the Reynolds number and the
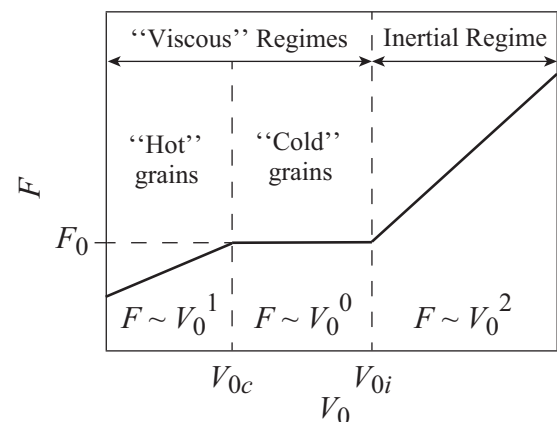

FIG. 5. Sketch of the evolution of the normalized drag force F in a granular packing as a function of velocity V_0 in a log-log plot.

Froude number $\text{Fr} = V_0/(gh)^{1/2}$: $\text{Fr} \sim \text{Re}^{1/2}(d_g/d)^{1/4}$. In the present experiments, the critical velocity should be $V_{0i} \sim 10^{-1}$ m.s^{-1}. This critical value is far from the available velocities of our present setup so that we cannot observe the inertial regime. This high-velocity inertial regime has however been observed by, e.g., Refs. [29,30] for velocities of these order of magnitude.

It is worth noting that the critical velocity V_{0c} varies with the vibration level, so that the drag force curve $F(V_0)$ can exhibit different shapes. Without external vibrations, V_{0c} vanishes so that $F(V_0)$ exhibits only two parts with first a plateau of constant value followed by a quadratic V_0^2 increase as considered by, e.g., Refs. [29,30]. For high enough external vibrations, V_{0c} tends toward V_{0i} (or higher) so that here again $F(V_0)$ exhibits only two parts with a first linear increase followed by a quadratic increase as in classical Newtonian fluids. For intermediate level of external vibrations, $0 < V_{0c} < V_{0i}$, $F(V_0)$ thus exhibits the three parts sketched in Fig. 5. These evolutions of the drag force $F(V_0)$ induced by the external vibration level are very close to the changes of the flow curves obtained by Ref. [7] for torque measurements in granular matter with controlled weak vibrations. Finally, we believe that for drag measurements in a small velocity range around V_{0c}, the $F(V_0)$ curve may appear as logarithmic as reported, e.g., by Refs. [20,28].

We think that our hydrodynamical modeling could be extended to other situations where the fluidization process results from the steady flow of a far wall [33–35]. For instance, in the case of the motion of the inner cylinder in the Couette geometry of Ref. [34], the radially decreasing bulk temperature should scale as $T_b \sim (\Omega R)^2$, where Ω and R are the rotation speed and the radius of the cylinder.

VI. CONCLUSION

In this paper, we focus on the transition from the well-known quasistatic regime of a drag force independent of velocity at low enough velocity to a second regime where the drag force is linear in velocity, which may be observed in the case where the granular packing is vibrated. Experimental data obtained with a bidimensional setup of a large intruder disk dragged into a horizontal assembly of smaller disks display the two regimes depending on the intruder disk velocity and vibration level of the overall packing. A hydrodynamical model is developed taking into account the two sources of fluidization—the local self fluidization by the disk motion and the global fluidization from the packing vibration—leading to grain fluctuations expressed in term of granular temperatures. The experimental data compare well with the model in the two different regimes. When the intruder velocity is smaller than a critical velocity, the drag force increases linearly with the velocity in a so-called "hot granular viscous regime" in which the fluidization induced by the intruder motion is negligible when compared to the fluidization of the overall packing. When the intruder velocity is larger than the critical velocity, the drag force does not depend anymore on the intruder velocity in a so-called "cold granular viscous regime" in which the fluidization induced by the overall packing is here negligible when compared to the fluidization induced by the intruder motion. This second regime which is the most observed for standard experimental situations should be followed by an "inertial regime" at even larger intruder velocity in which the drag force increases as the square of velocity.

[1] G. Reydellet and E. Clément, Phys. Rev. Lett. **86**, 3308 (2001).

[2] H. J. Melosh, *Oxford Monographs on Geology and Geophysics, No. 11. Research supported by NASA.* (Oxford University Press, New York, 1989), p. 253.

[3] R. D. Maladen, Y. Ding, C. Li, and D. I. Goldman Science **325**, 314 (2009).

[4] M. van Hecke, J. Phys. Condens. Matter **22**, 033101 (2010).

[5] C. Coulais, A. Seguin, and O. Dauchot, Phys. Rev. Lett. **113**, 198001 (2014).

[6] A. Seguin and O. Dauchot, Phys. Rev. Lett. **117**, 228001 (2016).

[7] J. A. Dijksman, G. H. Wortel, L. T. H. van Dellen, O. Dauchot, and M. van Hecke, Phys. Rev. Lett. **107**, 108303 (2011).

[8] F. Lechenault, O. Dauchot, G. Biroli, and J. P. Bouchaud, Europhys. Lett. **83**, 46003 (2008).

[9] D. L. Henann and K. Kamrin, Phys. Rev. Lett. **113**, 178001 (2014).

[10] Q. Zhang and K. Kamrin, Phys. Rev. Lett. **118**, 058001 (2017).

[11] M. Bouzid, M. Trulsson, P. Claudin, E. Clément, and B. Andréotti, Phys. Rev. Lett. **111**, 238301 (2013).

[12] M. Bouzid, A. Izzet, M. Trulsson, E. Clément, P. Claudin, and B. Andreotti, Eur. Phys. J. E **38**, 125 (2015).

[13] J. T. Jenkins and D. Berzi, Granul. Matter **14**, 79 (2012).

[14] D. Berzi and J. T. Jenkins, Soft Matter **11**, 4799 (2015).

[15] A. Seguin, C. Coulais, F. Martinez, Y. Bertho, and P. Gondret, Phys. Rev. E **93**, 012904 (2016).

[16] R. Albert, M. A. Pfeifer, A.-L. Barabási, and P. Schiffer, Phys. Rev. Lett. **82**, 205 (1999).

[17] I. Albert, P. Tegzes, B. Kahng, R. Albert, J. G. Sample, M. Pfeifer, A.-L. Barabási, T. Vicsek, and P. Schiffer, Phys. Rev. Lett. **84**, 5122 (2000).

[18] I. Albert, P. Tegzes, R. Albert, J. G. Sample, A. L. Barabási, T. Vicsek, B. Kahng, and P. Schiffer, Phys. Rev. E **64**, 031307 (2001).

[19] C. R. Wassgren, J. A. Cordova, R. Zenit, and A. Karion, Phys. Fluids **15**, 3318 (2003).

[20] R. Candelier and O. Dauchot, Phys. Rev. Lett. **103**, 128001 (2009).

[21] A. Seguin, Y. Bertho, P. Gondret, and J. Crassous, Europhys. Lett. **88**, 44002 (2009).

[22] J. F. Boudet and H. Kellay, Phys. Rev. Lett. **105**, 104501 (2010).

[23] A. Seguin, Y. Bertho, P. Gondret, and J. Crassous, Phys. Rev. Lett. **107**, 048001 (2011).

[24] A. Seguin, Y. Bertho, F. Martinez, J. Crassous, and P. Gondret, Phys. Rev. E **87**, 012201 (2013).

[25] F. Guillard, Y. Forterre, and O. Pouliquen, Phys. Rev. Lett. **110**, 138303 (2013).

[26] A. Seguin, A. Lefebvre-Lepot, S. Faure, and P. Gondret, Eur. Phys. J. E **39**, 1 (2016).

[27] O. Zik, J. Stavans, and Y. Rabin, Europhys. Lett. **17**, 315 (1992).

[28] G. A. Caballero-Robledo and E. Clément, Eur. Phys. J. E **30**, 395 (2009).

[29] Y. Takehara, S. Fujimoto, and K. Okumura, Europhys. Lett. **92**, 44003 (2010).

[30] Y. Takehara and K. Okumura, Phys. Rev. Lett. **112**, 148001 (2014).

[31] I. Albert, J. G. Sample, A. J. Morss, S. Rajagopalan, A.-L. Barabási, and P. Schiffer, Phys. Rev. E **64**, 061303 (2001).

[32] R. Harich, T. Darnige, E. Kolb, and E. Clément, Europhys. Lett. **96**, 54003 (2011).

[33] K. Nichol, A. Zanin, R. Bastien, E. Wandersman, and M. van Hecke, Phys. Rev. Lett. **104**, 078302 (2010).

[34] K. A. Reddy, Y. Forterre, and O. Pouliquen, Phys. Rev. Lett. **106**, 108301 (2011).

[35] E. Wandersman and M. van Hecke, Europhys. Lett. **105**, 24002 (2014).

[36] C. Coulais, R. P. Behringer, and O. Dauchot, Europhys. Lett. **100**, 44005 (2012).

[37] C. Coulais, R. P. Behringer, and O. Dauchot, Soft Matter **10**, 1519 (2014).

[38] N. Menon and D. J. Durian, Phys. Rev. Lett. **79**, 3407 (1997).

[39] A. Seguin, Y. Bertho, and P. Gondret, Phys. Rev. E **78**, 010301 (2008).

[40] M. B. Stone, R. Barry, D. P. Bernstein, M. D. Pelc, Y. K. Tsui, and P. Schiffer, Phys. Rev. E **70**, 041301 (2004).

[41] J. T. Jenkins and S. B. Savage, J. Fluid Mech. **130**, 187 (1983).

[42] W. Losert, L. Bocquet, T. C. Lubensky, and J. P. Gollub, Phys. Rev. Lett. **85**, 1428 (2000).

[43] L. Bocquet, W. Losert, D. Schalk, T. C. Lubensky, and J. P. Gollub, Phys. Rev. E **65**, 011307 (2001).

[44] D. Chehata, R. Zenit, and C. R. Wassgren, Phys. Fluids **15**, 1622 (2003).